ACS APPLIED ENERGY MATERIALS

www.acsaem.org Article

Interfacial Charge Transfer and Zinc Ion Intercalation and Deintercalation Dynamics in Flexible Multicolor Electrochromic Energy Storage Devices

Chunjian Wang, Xinlei Zhang, Sheng Liu, Hongliang Zhang,* Qiang Wang, Chengli Zhang, Junhua Gao, Lingyan Liang, and Hongtao Cao*

Cite This: *ACS Appl. Energy Mater.* 2022, 5, 88−97 Read Online

ACCESS | Metrics & More | Article Recommendations | Supporting Information

ABSTRACT: Bifunctional electrochromic devices integrating electrochromism and energy storage have attracted extensive attention in recent years. Here, zinc-ion-intercalation-based multicolor electrochromic energy storage devices (EESDs) based on a free-standing Zn^{2+}-based polymeric electrolyte membrane (ZPEM) and a nanocrystal-in-glass V_2O_5 thin film were constructed. Evolution of the interlayer spacing, V−O-related bonds, and chemical compositions of the V_2O_5 thin films with zinc ion intercalation and deintercalation is elaborated in a liquid $Zn(CF_3SO_3)_2$-propylene carbonate (PC) electrolyte. Impressively, highly reversible multi-electrochromism among greenish-blue, yellowish-green, greenish-yellow, faint-yellow, yellowish-orange, and reddish-orange colors is observed in both flexible V_2O_5 thin films and flexible ZPEM/V_2O_5/indium tin oxide (ITO) EESDs, which enjoy the benefits from the free channel originating from the large interlayer spacing, the buffering effect of the amorphous phase in the host nanocrystal-in-glass V_2O_5 matrix, the robust electrostatic interactions between the host V_2O_5 and guest Zn^{2+}, and Faradaic redox reactions at the Zn^{2+}/V_2O_5 active interface. The flexible multicolor EESD based on zinc ion intercalation and deintercalation exhibits remarkable electrochromic and energy storage performance with a high transmittance modulation of 57.88%, an excellent coloration efficiency of 36.91 $cm^2\ C^{-1}$, a superior specific capacitance of 51 $\mu F\ cm^{-2}$, an enhanced rate capacity, and a pseudocapacitive feature, making it a promising candidate for cost-efficient, environmentally friendly, and bifunctional electrochromic devices.

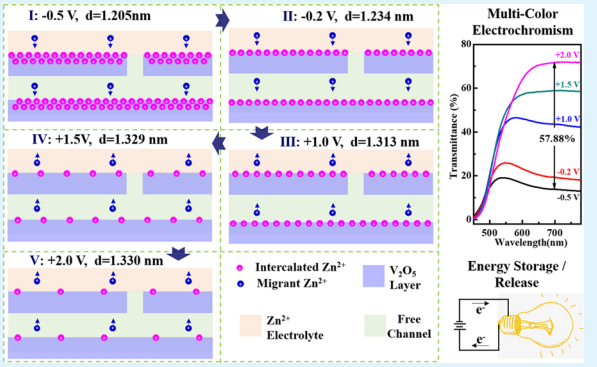

KEYWORDS: *zinc-ion intercalation, multicolor electrochromism, vanadium pentoxide, electrochromic energy storage devices, flexible electrochromic devices*

INTRODUCTION

To meet the future demand of portable electronics, there is an urgent need to develop flexible, light-weighted, and high-performance multifunctional energy storage devices having a higher power density and large energy capacity.[1−3] Electrochromic energy storage devices (EESDs) integrating electrochromism and energy storage show increasingly bright prospects. This combination achieves the advantages of the two related electrochemical applications. On the one hand, charges can be stored in EESDs when the electrochromic devices (ECDs) change their color; on the other hand, the state of energy storage can be inspected by simple glances.[4] Over the past few years, electrochromic supercapacitors (ECSs) have attracted extensive interest as a state-of-the-art energy storage device due to their unique advantage when compared to the conventional storage media such as batteries and electrostatic capacitors.[5] A typical example is that an electrochromic supercapacitor (ECS) composed of WO_3 and NiO can deliver a high-performance operating regime, which provides a large areal capacitance (~14.9 mF cm^{-2}), an excellent Coulombic efficiency (~99%), an ultrahigh charging/discharging cyclic stability (>10 000 cycles), and good self-discharging durability.[6] However, the energy density falls short of practical application because of the electrostatic-charge storage mechanism.[7] This problem can be tackled using pseudocapacitive materials, like transition-metal oxides or conductive polymers, because of their high theoretical capacity, which can enhance the energy density.[8−10] For instance, a nanocomposite NiO-TiO_2 thin film of a polycrystalline-in-glass electrolyte matrix has been demonstrated to manifest an excellent reversible electro-optic durability and a large charge/

Received: August 18, 2021
Accepted: December 7, 2021
Published: December 21, 2021

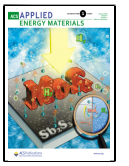

https://doi.org/10.1021/acsaem.1c02508
ACS Appl. Energy Mater. 2022, 5, 88−97

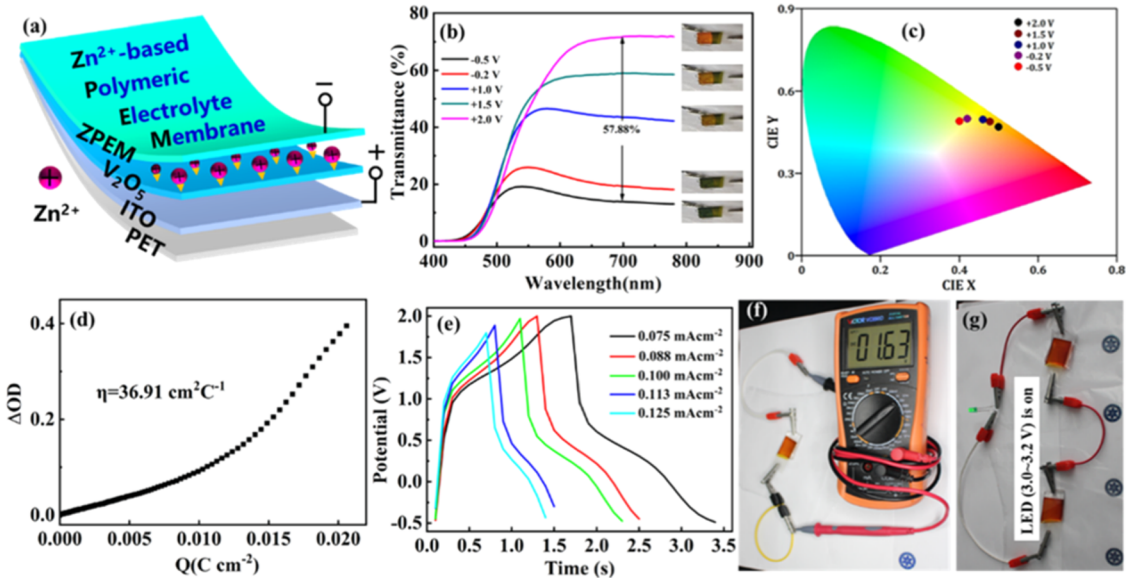

Figure 1. (a) Schematic illustration and (b) *ex situ* optical transmittance spectra of Zn^{2+}-based polymeric electrolyte membrane. Inset: digital photographs of the V_2O_5 electrochromic device in various colored and bleached states. (c) Commission Internationale de L'Eclairage (CIE) coordinates of the flexible ZPEM/V_2O_5/indium tin oxide (ITO) EESD in various colored states from −0.5 to +2.0 V. (d) *In situ* optical density variation *versus* charge density for the EESD. (e) Galvanostatic charge/discharge (GCD) curves of the flexible ZPEM/V_2O_5/ITO EESD at different current densities from 75.0 to 125.0 μA cm^{-2}. (f) Digital photograph of the open-circuit voltage of a single fully bleached (+2.0 V) ZPEM/V_2O_5/ITO EESD. (g) Digital photographs of the brightest state of the green light-emitting diode (LED) driven by a couple of the fully bleached (+2.0 V) ZPEM/V_2O_5/ITO EESDs in series.

discharge capacity.[11] Recently, the concurrent electrochromic and pseudocapacitive roles of a poly(3,4-ethylenedioxypyrrole) (PEDOP)−Au@WO_3 hybrid film in 1-butyl-3-methyl imidazoliumtriflate electrolyte have been established, in the hope of providing a new electrochromic approach for coupling this conducting polymer with electroactive oxide nanostructures.[12] Unfortunately, all of the previously mentioned methods suffer from some serious limitations. For example, despite the wide usage of tungsten oxide in electrochromic supercapacitors, the monochromic change from transparency to blue limits the practical application.[13] Thus, V_2O_5-based materials have been brought into view as the most propitious candidates for electrochromic supercapacitors. For instance, a novel aqueous Zn−V_3O_7 electrochromic battery display using synthesized colloidal V_3O_7 nanoparticles (cathodes) and Zn foils (anodes) demonstrates reversible color change (yellow, grayish-blue, and half yellow−half grayish-blue images) and partial energy retrieval functions.[14] In addition to that, it has been reported that the layered structure of V_2O_5 enjoys a variety of advantages, such as shortening the switching time by offering a free channel between layers and increasing the capacity of the capacitor by offering more voids for intercalation, thus significantly enhancing the electrochemical performance.[15−18] Also, Li-ion pseudocapacitors suffer from several restrictions, such as the rigidity of the assembling environment, the flammability and toxicity of organic electrolyte solutions, and the potential risk of the Li source.[19] Recent studies reported by Li et al. also support the hypothesis that the highly efficient intercalation of Al ions into layered single-crystal $W_{18}O_{49}$ electrodes with a hierarchically porous structure and wide lattice spacing results in high-performance electrochromic supercapacitor devices based on electrochemical storage.[20] The evidence presented thus far supports the idea that trivalent Al-ion-intercalation-based electrochromic devices benefit from high capacity, small ionic radius, cost-effectiveness, and safety.[21,22] However, aluminum ions usually lead to many undesirable ionic behaviors. The study showed that Al^{3+} has been proven to have a stronger inhibition effect than Zn^{2+} because of its larger hydrated ionic radius and higher binding capacity.[23] In addition, Zn^{2+} has a small ionic radius of 0.074 nm, comparable to that of Li^+ (0.069 nm), while the electrostatic interaction is stronger between Zn^{2+} and the lattice of the host material, making them promising for electrochromic energy storage devices.[24] However, to the best of our knowledge, an active interface of a V_2O_5/Zn^{2+}-based electrolyte has not been applied in multicolor electrochromic energy storage devices, and the understanding of interfacial charge transfer and zinc ion intercalation and deintercalation dynamics in V_2O_5 electrochromic thin films is very limited.

In this paper, a novelly assembled flexible electrochromic energy storage device (EESD) combining two advantageous materials of zinc ions and a layered V_2O_5 thin film shows a multicolor electrochromism and a pseudocapacitive energy storage feature by introducing a free-standing Zn^{2+}-based polymeric electrolyte membrane (ZPEM) as the electrolyte layer, as shown in Figure 1. Also, an overall understanding of the sources of the enhanced interfacial charge transfer and the dynamics of zinc ion intercalation/deintercalation in a nanocrystal-in-glass V_2O_5 thin film with a layered structure is uncovered.

EXPERIMENTAL SECTION

The V_2O_5 thin films were synthesized using a two-electrode electrochemical deposition system with an indium tin oxide (ITO)/poly(ethylene terephthalate) (PET) substrate as the working electrode and a Pt sheet as the counter electrode. The square resistance and thickness of the ITO thin film electrode are estimated to be 80−100 Ω sq^{-1} and 100−150 nm, respectively. First, 0.25 g of V_2O_5 (analytically pure 99.5%) was added to 8 mL of deionized water to form a yellowish slurry liquid. Then, 3 mL of a 30 wt % solution of H_2O_2 was added to the slurry under continuous stirring for 20 min.

https://doi.org/10.1021/acsaem.1c02508
ACS Appl. Energy Mater. 2022, 5, 88−97

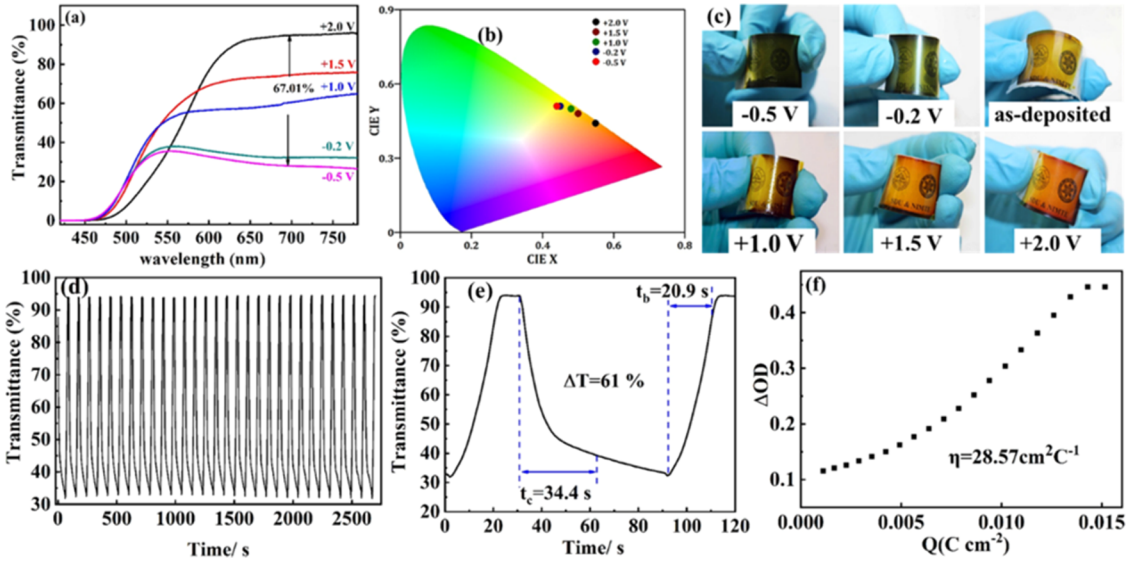

Figure 2. (a) *Ex situ* optical transmittance spectra. (b) CIE coordinates of the as-deposited V_2O_5 thin films and the V_2O_5 thin films in various colored states of +2.0, +1.5, +1.0, −0.2, and −0.5 V. (c) Digital photographs. Copyright 2021 Chinese Academy of Sciences. (d, e) *In situ* time-dependent optical transmittance spectra at a wavelength of 700 nm (−0.5 V for 30 s/+2.0 V for 60 s). (f) *In situ* optical density variation *versus* charge density for the V_2O_5 thin films.

After that, a brick-red precursor formed, and 40 mL of deionized water was added to the precursor ultrasonication for 15 min. Then, the solution was aged for 1 week. The electrodeposition solution was obtained by dispersing 5 mL of aged brick-red precursor in 50 mL of anhydrous ethanol. Subsequently, the V_2O_5 thin films were deposited using a potentiostatistical method, which applies a fixed potential of 8.0 V at 60 °C for 8 min. These electrochemically deposited films were subjected to a final drying procedure in which the temperature was 60 °C over 12 h in air.

The free-standing Zn^{2+}-based polymeric electrolyte membrane (ZPEM) was synthesized *via* a solution process. $Zn(CF_3SO_3)_2$ (0.4 mol L^{-1}), 15.6 g of acrylamide monomer (AM, 2.2 mol L^{-1}), *N*,*N*′-methylenebisacrylamide (MBAA, 0.06% by weight of AM), ammonium persulfate (AP, 0.17% by weight of AM) as the initiator, and *N*,*N*,*N*′,*N*′-tetramethylenediamine (TEMED, 0.15% by weight of AM) as the crosslinking accelerator were orderly dissolved in 100 mL of deionized water for 30 min at room temperature (RT) stirred by a magnetic stirrer. Subsequently, the obtained solution was poured into the closed parallel plates with a space distance of ∼3 mm to form a transparent free-standing ZPEM for 2 h at RT. The preparation process is similar to that of the Li^+-based gelatin-based solid electrolyte for the complementary ECDs elsewhere.[25]

The viscous transparent free-standing ZPEM was directly bonded on the synthesized V_2O_5/ITO/PET for performance assessment in the flexible ZPEM/V_2O_5/ITO ECDs. From the point of device geometry, the ZPEM/V_2O_5/ITO ECDs have the simplest structure, where the ZPEM can serve as a three-in-one layer incorporating the electrolyte layer, the ion storage layer, and the transparent conducting electrode at the same time, compared with conventional layer-by-layer assembled complementary electrochromic devices.

Measurements of X-ray diffraction (XRD) profiles were obtained in a Bruker D8 Advance ($\theta/2\theta$ coupled geometry) through an X-pert powder XRD system with Cu Kα radiation (λ = 0.154178 nm). The V_2O_5 thin films were further characterized by field emission scanning electron microscopy (FESEM, S4800), Raman spectra (Renishaw inVia Raman microscope using excitation laser at a wavelength of 633 nm), and high-resolution transmission electron microscopy (HRTEM, JEOL 2100). The *ex situ* transmission spectra of the V_2O_5 thin films were measured in a UV−vis−IR spectroscopy (PerkinElmer Lambda 950) in the fully colored and fully bleached states. The electrochemical performance of the V_2O_5 thin films was measured at RT on an electrochemical workstation (CHI660D, Chenhua, Shanghai). The measurement was carried out in a three-electrode system, a KCl-saturated Hg/$HgCl_2$ electrode as the reference electrode, a Pt foil as the counter electrode, and the V_2O_5 thin films on the ITO/PET substrates as the working electrode in a liquid $Zn(CF_3SO_3)_2$-PC electrolyte, which was synthesized by dissolving 0.4 M $Zn(CF_3SO_3)_2$ in propylene carbonate (PC). *In situ* transmittance spectra were obtained through an electrochemical workstation and UV−vis−IR spectroscopy. Cyclic voltammetry (CV) and chronoamperometry (CA) measurements were performed with a CHI660c electrochemical workstation between −0.5 and +2.0 V at RT. The galvanostatic charge/discharge (GCD) curve method was used to calculate the area-specific capacitance of the electrode materials. The electrochemical impedance spectra (EIS) were measured in an electrochemical workstation (Zennium, IM6) at a frequency ranging from 100 mHz to 100 kHz with a potential amplitude of 10 mV under a DC bias from 0 to −0.5 V. *Z*-View software was used to fit EIS data in the equivalent circuit.

RESULTS AND DISCUSSION

Figure 2a displays *ex situ* transmittance spectra of the V_2O_5 thin films in various colored and bleached states at a wavelength ranging from 380 to 780 nm. In general, the V_2O_5 thin films exhibit reddish-orange and greenish-blue colors at oxidation and the highest reduced state, which can be defined as the bleached and colored states at positive and negative voltages, respectively. A high optical transmittance modulation (ΔT) of 67.01% is observed at λ = 700 nm. And the highest transmittance of up to 94.86% is obtained at a positive voltage of +2.0 V. A further color analysis based on the Commission Internationale de L'Eclairage (CIE) system of colorimetry for the V_2O_5 thin films in different states is presented in Figure 2b. In terms of the CIE coordinate, an approximate linear distribution is observed from the bleached state (+2.0 V) to the colored state (−0.5 V) in the CIE with an *X* range of 0.55−0.47. Figure 2c shows the digital photographs of the as-deposited V_2O_5 thin film and the films in various states. The V_2O_5 thin films display a reversibly switchable multi-electrochromic characteristic with several colors such as greenish-blue, yellowish-green, greenish-yellow, faint-yellow, yellowish-orange, and reddish-orange, consistent with that of the CIE system. Figure 2d,e shows *in situ* time-dependent

https://doi.org/10.1021/acsaem.1c02508
ACS Appl. Energy Mater. 2022, 5, 88−97

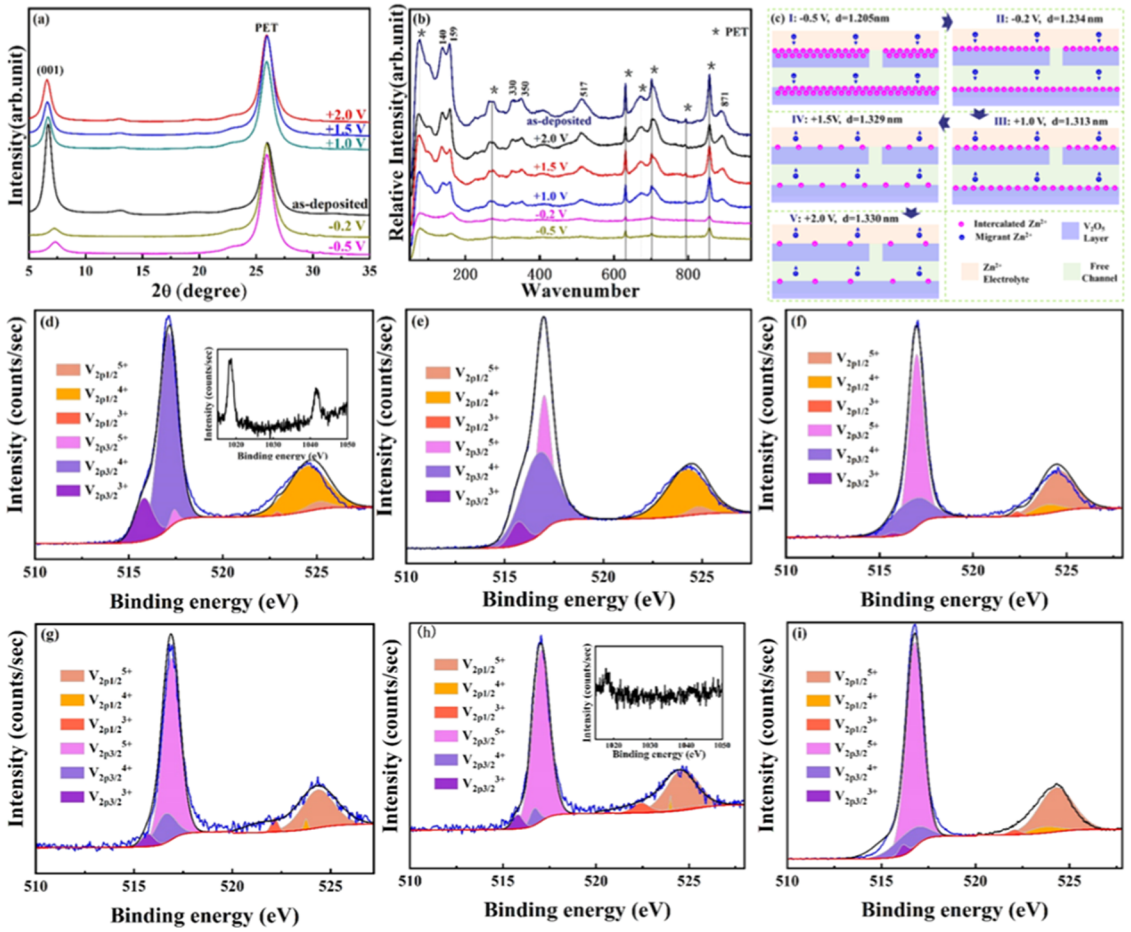

Figure 3. (a) XRD patterns and (b) Raman spectra of the as-deposited V_2O_5 thin films and the V_2O_5 thin films in various colored and bleached states of +2.0, +1.5, +1.0, −0.2, and −0.5 V. (c) Schematic diagram of the evolution of the intercalation/deintercalation of zinc ions into the host layered V_2O_5 at various potentials. Resolved XPS spectra of V_{2p} from the V_2O_5 thin films in various colored states of (d) −0.5 V, (e) −0.2 V, (f) +1.0 V, (g) +1.5 V, (h) +2.0 V, and (i) the as-deposited V_2O_5 thin films. Inset: resolved XPS spectra of Zn V_{2p} of −0.5 and +2.0 V.

transmittance spectra at λ_{633nm} for the as-deposited V_2O_5 thin films. The maximum transmittance modulation (ΔT) of the V_2O_5 thin films in a liquid $Zn(CF_3SO_3)_2$-PC electrolyte was measured to be 61% when applying a voltage of −0.5/+2.0 V for 60/30 s, respectively. No distinct variation in the maximum optical transmittance modulation is observed after 30 cycles. The good cycling stability can be owed to the layered and nanocrystal-in-glass structures, which facilitate the insertion and extraction of Zn^{2+} and alleviate the stress caused by these processes.[26] It is well known that switching time, prescribed as the time required for a 90% change to occur in the full transmittance modulation, is an important parameter for the practical applications of ECDs. In our case, the switching times are obtained at a wavelength of 633 nm. The coloration/bleaching time of the V_2O_5 thin films in a liquid $Zn(CF_3SO_3)_2$-PC electrolyte is measured to be 20.9/34.4 s. Such short colored/bleached EC response time can be chiefly attributed to the large interlayer space of more than 1.20 nm in the layered structure. This unique structure shortens the ion diffusion and electron transportation distance, leading to a shorter switching time.[22] It is almost certain that the utilization of the Li-ions, which have a high ion diffusion coefficient and high electrical conductivity, can improve the coloration/bleaching speed of the electrochromic thin films. Thus, the obtained switching times in the zinc ion electrolyte are significantly higher than the reported values in a lithium-ion electrolyte.[27] The coloration efficiency (CE) is defined as the change of optical density change (ΔOD) by per unit charge (ΔQ) insertion or exaction, which can be calculated by the following equation[28]

$$CE = \Delta OD/q = \log(T_{bleached}/T_{colored})/q \quad (1)$$

where Q is the inserted (extracted) charge per unit area and $T_{bleached}$ and $T_{colored}$ represent the transmittance of the V_2O_5 film in the bleached and colored states, respectively. The CE is estimated to be 28.57 $cm^2\ C^{-1}$ from the slope of the plots of ΔOD *versus* the charge density, as shown in Figure 2f.

Figure 3a shows the XRD patterns of the as-deposited V_2O_5 thin films and the V_2O_5 thin films in various colored states of −0.5, −0.2, +1.0, +1.5, and +2.0 V. The two distinct diffraction peaks centered at ∼6.82 and ∼26.16° correspond to the (001) crystal planes of the V_2O_5 thin films, which is the characteristic of the layered structure and the diffraction peak of the PET substrate, respectively.[29] The layered structure and nanocrystal-in-glass characteristic of the V_2O_5 thin films can be further supported by the HRTEM and FESEM images, as shown in Figure S1. The cross-sectional images (Figure S1a) confirm that the V_2O_5 thin film possesses a multilayered and stacked characteristic, and the thickness of the film is estimated to be ∼2.91 μm. In Figure S1b, the smooth and crack-free surface of the V_2O_5 thin films embedded with uniformly distributed V_2O_5 nanocrystal can be observed. The flaky

https://doi.org/10.1021/acsaem.1c02508
ACS Appl. Energy Mater. 2022, 5, 88−97

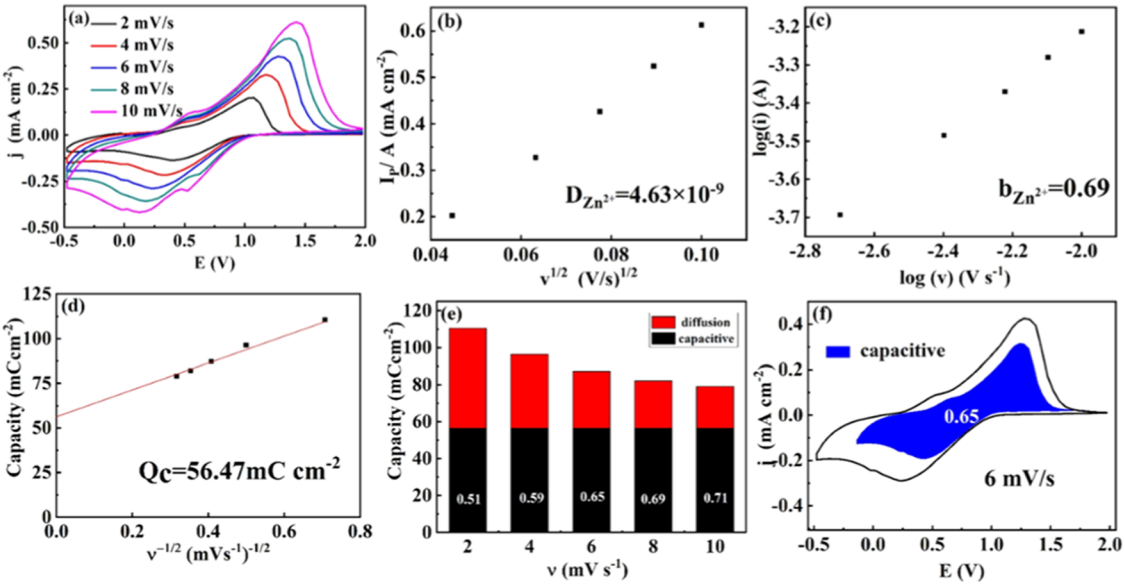

Figure 4. (a) Cyclic voltammograms of the as-deposited V_2O_5 thin films with the applied potential from −0.5 to +2.0 V at different scan rates from 2 to 10 mV s^{-1}. (b) Dependence between the peak current densities (I_p) and the square root of scan rate ($v^{1/2}$). (c) Power-law dependence between the peak current and the logarithm of scan rate. (d, e) Separation of the contributions to the capacitive- and diffusion-controlled processes of the V_2O_5 thin films in Zn^{2+} electrolytes at different scan rates. (f) Capacitive storage (blue) and the corresponding ratio at 6 mV s^{-1}.

structure is further confirmed by the TEM results of the V_2O_5 thin films peeled off from the ITO/PET substrate (Figure S1c). The selected area electron diffraction (SAED) pattern shows two diffraction rings corresponding to the (701) and (510) planes of the polycrystalline V_2O_5, respectively. The HRTEM image (Figure S1d) indicates that an amorphous phase is embedded with nanocrystals with three distinct values for interplanar spacings of 0.207, 0.217, and 0.183 nm, corresponding to the (701), (020), and (121) lattice planes of V_2O_5 (PDF # 892483), respectively. The findings from these experiments indicate that the V_2O_5 thin film enjoys the benefits of the layered and nanocrystal-in-glass structures. Moreover, the predominantly amorphous nature of the V_2O_5 thin films is exhibited, similar to the previously published work.[30,31] According to the Bragg formula,[32] the interlayer spacing of the V_2O_5 thin film in the colored states of −0.5, −0.2, +1.0, +1.5, and +2.0 V is calculated to be, respectively, 1.205, 1.234, 1.313, 1.329, and 1.330 nm, much larger than the Zn^{2+} radius of 0.074 nm.[33,34] Such a large interlayer spacing can provide a free channel for zinc ion intercalation and deintercalation.[29] It is worth pointing out that the change in the interlayer spacing caused by the intercalation of guest Zn^{2+} into host V_2O_5 can depend on a certain "comprehensive effect" which stems from the electrostatic force and the amount of substance per unit volume. For such a sufficiently large interlayer space, the potential volume expansion caused by the intercalation of a limited number of small radius Zn^{2+} ions is considered to be negligible compared to the increase in the interlayer spacing caused by the electrostatic force. Thus, the gradual increase in the interlayer spacing with applied voltages from −0.5 to +2.0 V is due to the deintercalation of both zinc ions and electrons since the electrostatic force is gradually reduced during the extraction, similar to those in the $Li^+-V_2O_5$ system.[35] The absence of a distinct structural difference in the V_2O_5 thin film between the intercalation and deintercalation of Zn^{2+} suggests the stability of the layered structure. Raman spectra of the as-deposited V_2O_5 thin film and the V_2O_5 thin films in various coloration states are shown in Figure 3b. A summary of the observed bands of V_2O_5 and their attributions is provided in Table S1. Raman peak located at 140 cm^{-1} in the lower frequency is assigned to the stretching mode of $(V_2O_2)_n$, which corresponds to the chain translation.[36] The vibrational modes of V_2O_5[29,37] bonds have been found to be at 159 and 350 cm^{-1} for the as-deposited and colored V_2O_5 thin films. The peaks at 330 and 517 cm^{-1} are, respectively, ascribed to the bending vibration of the $V-O_3$ bonds' stretching mode[29] and the triply coordinated oxygen V_3-O,[38] which stems from an edge-shared oxygen atom in common to three pyramids. The doubly coordinated oxygen V_2-O stretching and bending vibration mode contribute to the peak at 871 cm^{-1}, derived from corner-shared oxygen in common to two pyramids.[39] Overall, the vibrational modes of $(V_2O_2)_n$, $V-O_3$ bonds, V_2O_5 phase, and V_2-O are Raman-active in the as-deposited V_2O_5 thin films and the V_2O_5 thin films in the colored states (+1.0, +1.5, and +2.0 V). In contrast, these modes are almost always not observed for the V_2O_5 thin films in various colored states (−0.2 and −0.5 V). These results indicate that zinc-ion-intercalation makes the vibrational modes of $(V_2O_2)_n$, $V-O_3$ bonds, V_2O_5 phase, and V_2-O silent, which can be induced by defects and impurities due to the dominant reduction reaction of the interface between the V_2O_5 electrodes and the Zn^{2+} electrolyte at the applied negative potentials. To clarify the mechanism of the mechanical action and charge transfer of zinc ion intercalation and deintercalation, Figure 3c illustrates a schematic diagram of the evolution of the layered V_2O_5 thin films with zinc ion intercalation/deintercalation at the applied negative/positive potentials, respectively. A possible explanation for this might be that the intrinsic layered and nanocrystal-in-glass structural characteristics of the V_2O_5 host cannot distinctly be altered by zinc ion intercalation and deintercalation. As clearly seen in Figure 3c, the increase of voltage from −0.5 to +2.0 V leads to a gradual increase in the interlayer spacing due to the gradual deintercalation and the transfer of more Zn^{2+} ions from the crystal lattice, consistent with the results of XRD analysis. These results are similar to those reported by Jin et al.[40] Moreover, in support of the

https://doi.org/10.1021/acsaem.1c02508
ACS Appl. Energy Mater. 2022, 5, 88−97

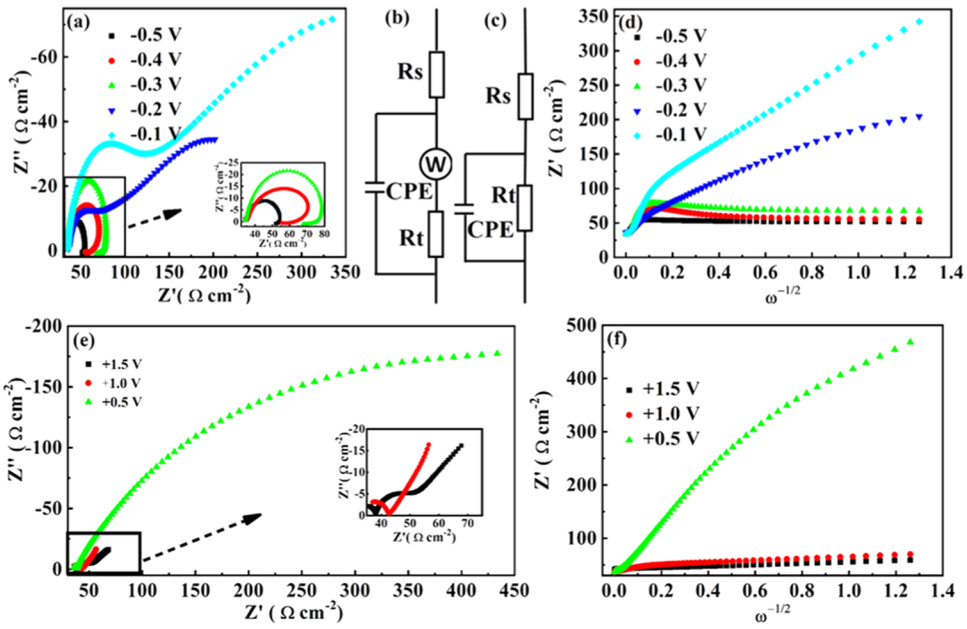

Figure 5. (a) Nyquist diagrams at various negative potentials from −0.1 to −0.5 V. (b, c) Equivalent circuits for analyzing the impedance data. (d) Diagrams of the correlation between the real impedance (Z') and the angular frequency ($\omega = 2\pi f$) at a low-frequency. (e) Nyquist diagrams at various positive potentials from 0.5 to 1.5 V, and (f) the real impedance (Z') *versus* angular frequency ($\omega = 2\pi f$) dependency plots in the low-frequency region.

widely held view that electrochromic energy storage devices (EESDs) can achieve both optical modulation and energy storage/release at the same time, both interface optical properties and charge storage capacitance appear to be manipulated by zinc ion intercalation and deintercalation, which is a promising approach for flexible multicolor EESDs. To further illustrate the variation in chemical compositions of the interface between the V_2O_5 thin films and the zinc ion electrolyte, all V_{2p} spectra of the as-deposited V_2O_5 thin film and the V_2O_5 thin films in various coloration states measured by X-ray photoelectron spectroscopy (XPS) are given in Figure 3d−i. Also, the quantitatively detailed XPS results are summarized in Table S2. For the as-deposited V_2O_5 thin film, the V^{5+}, V^{4+}, and V^{3+} components are calculated to be 83.89, 4.46, and 11.65% (atomic percentage, atom %), respectively, in good agreement with that observed in the previous report.[15] The content of the V^{5+} component increases from 4.29 to 90.40% as the applied voltage increases from −0.5 to +2.0 V, and accordingly, V^{4+} and V^{3+} components decrease. This demonstrates that V^{4+} and V^{3+} in the interface of the V_2O_5 thin films can be oxidized into V^{5+} due to the Zn^{2+}−V_2O_5 oxidation reaction, similar to the Li^+−V_2O_5 system in the previous work.[41] In fact, it is demonstrated that V^{4+} and V^{3+} are reduced to V^{5+} for the Zn^{2+}−V_2O_5 battery.[42] Furthermore, the Zn_{2p} component is almost always observed for the V_2O_5 thin films in various colored states (−0.2 and −0.5 V) but is otherwise undetected in various bleached states (+1.0, +1.5, and +2.0 V), as shown in the inset of Figure 3d,h. The findings indicate that zinc ions can reversibly insert/extract into/from the active interface between the V_2O_5 electrodes and zinc ion electrolyte at the applied negative/positive potentials, similar to the Zn^{2+}−V_2O_5 battery.[43]

Figure 4a displays the cyclic voltammetry (CV) of the V_2O_5 thin films at various scan rates in the three-electrode testing system in a liquid 0.4 M $Zn(CF_3SO_3)_2$-PC electrolyte. The two pairs of redox peaks in the cyclic voltammogram can be considered as a reversible redox process accompanied by the double insertion/extraction of Zn^{2+} ions and electrons, which can be conveyed by the following reversible Faradaic redox reaction: $V_2O_5 + xZn^{2+} + 2xe^- \leftrightarrow Zn_xV_2O_5$, consistent with the previous report.[46] As the scan rate increases from 2 to 10 mV s^{-1}, the separation between the two redox peaks increases significantly. This indicates that the polarization effect of the electrode causes an increase of the internal diffusion resistance of the electrode and limits the rate of double injection/extraction of Zn^{2+} and electrons into/from the V_2O_5 matrix, as stated in the previous work.[44] As reported previously, the ion diffusion coefficient and ion diffusion distance essentially affect the switching speed of electrochromic devices.[22] The diffusion coefficient (D) obeys the Randles−Sevcik law, which can be calculated from the equations as follows

$$I_p = 2.72 \times 10^5 \times n^{3/2} \times A \times D^{1/2} \times C_0 \times V^{1/2} \quad (2)$$

where I_p represents the peak current (A), n is the number of electrons (2), A is the working electrode area (cm^2), C_0 is the concentration of the electrolyte (mol cm^{-3}), and v is the scan rates (mV s^{-1}).[45] By considering the CV curves, the obtained Zn^{2+} diffusion coefficient (D) in intercalation and deintercalation processes is 4.63×10^{-9} (Figure 4b). Such a large value can be attributed to the large interlayer spacing of the V_2O_5 thin films, small radius, and large electrostatic forces of the guest divalent zinc ions and water-lubricated intercalation in potential $V_2O_5{\cdot}nH_2O$, which boosts the transfer of charges, promotes the infiltration of electrolyte, and alleviates the structural distortion of the V_2O_5 films during zinc ion intercalation.[8,24,46] To characterize the kinetics of charge storage in the V_2O_5 thin films, the relation between peak current (i) *versus* scan rate (v) was studied in the three-electrode system. The total stored charge of the V_2O_5 thin films can be divided into two parts, which are the contributions of the capacitive effect and diffusion.[44,47] To identify the

https://doi.org/10.1021/acsaem.1c02508
ACS Appl. Energy Mater. 2022, 5, 88−97

capacitive effects and diffusion-controlled process, the CV data were analyzed according to the power-law relationship

$$i = a\nu^b \text{ or } \log(i) = \log(a) + b\log(\nu) \quad (3)$$

where a and b are adjustable parameters. The "b" value is determined by the slope of the plot of $\log(i)$ *versus* $\log(\nu)$ for cathodic or anodic peaks, which describes the intrinsic kinetics of the charge storage mechanism.[47] In general, the kinetics of the system converges to be diffusion-controlled if the "b" value is 0.5; alternatively, the kinetics of the system is fast enough to be a capacitive response if the "b" value is close to 1.[42,48] As shown in Figure 4c, the "b" value of the line is estimated to be 0.69, revealing that the high-capacity contribution arises from pseudocapacitive charge storage. Moreover, Trasatti's analysis is another powerful tool to analyze the capacitive and diffusive charge storage contributions, which is dependent on the scan rates.[47] According to the diffusion law, Q, which can be calculated by the following equation, is linear *versus* the reciprocal of the square root of the scan rate[8,41,46,47]

$$Q(\nu) = Q_c + k \times \nu^{-1/2} \quad (4)$$

The diffusion-dominated behaviors could be nearly eliminated when the ν value becomes an infinitely large number, which induces the extrapolated largest capacitive storage by extrapolation. Q_c, calculated to be approximately 56.47 mC cm^{-2}, is determined by the intercept of the fitting line, as presented in Figure 4d. Figure 4e shows the calculated distribution of capacitive charge and diffusion-controlled charge in V_2O_5 thin films at various scan rates from 2 to 10 mV s^{-1}. With the increase of the scan rates, the capacitive component of the total charge increases from 51% at 2 mV s^{-1} to 71% at 10 mV s^{-1}, aligning with the "b" values mentioned above. At a fast scan rate, the surface capacitive contribution becomes more dominant, whereas at a low scan rate, the diffusive contribution is non-negligible, as there is adequate time to allow ions to diffuse into the inner region.[47] The proportion of capacitive charge and diffusion-controlled charge of the V_2O_5 thin film at a scan rate of 6 mV s^{-1} is presented in Figure 4f. The blue part represents the capacitive contribution, while the diffusion effect is related to the other part.

To assess the electrochemical properties of the V_2O_5 electrochromic thin film, the electrochemical impedance spectra (EIS) were obtained using a three-electrode system. Figure 5 depicts Nyquist and the plots of the real impedance (Z') *versus* angular frequency ($\omega = 2\pi f$) dependency in the low-frequency region at various potentials. As presented in Figure 5b,c, EIS data were simulated by the corresponding typical equivalent circuits.[9,49] CPE represents constant phase elements, "W" represents the Warburg impedance of ionic diffusion in the low-frequency zone, and R_s is a series resistance in the electrolyte regime, respectively.[50,51] A depressed semicircle in the high-frequency region and an inclined line in the low-frequency region are observed in the Nyquist plots at negative potentials of −0.1 and −0.2 V, respectively, which corresponds to the charge-transfer resistance (R_{ct}) at the interface of the V_2O_5 electrode/zinc ion electrolyte and Warburg impedance, similar to the results of Li ions within the V_2O_5 electrode.[52] It can be seen that the increased negative potentials of −0.1 to −0.5 V result in a decrease in the magnitude of the low-frequency semicircle and the charge-transfer resistance 442.8−84.2 Ω, as listed in Table S3, which can be reconciled with a chemical reaction that becomes more intense at high potentials. Similarly, the value of the observed charge-transfer resistance decreases from 2392 to 39.1 Ω as a result of the increased positive potentials of +1.0 to +1.5 V (Table S3). These results can be chiefly ascribed to an electrochemical reaction of the electrode−material interface,[53] in good accordance with the transition from the conductor ($Zn_xV_2O_5$) to semiconductor (V_2O_5). Generally, a CPE-n (the exponent of CPE) of 0.5 is allocated to a semi-infinite diffusion and 1 to an ideal capacitor (surface-controlled). In our case, CPE-n of the bleached V_2O_5 thin films in the Zn^{2+} electrolyte at different potentials is calculated to be between 0.5 and 1, indicating the contribution of both semi-infinite diffusion and surface-controlled process to the electrochemical reaction, similar to the previous report.[22] These results further confirm the capacitive and diffusive charge storage contributions as indicated by the "b" values above. According to the dependence of the angular frequency ($\omega = 2\pi f$) on real impedance (Z) in the low-frequency region (Figure 5b,d), the increased potentials of both −0.1 to −0.5 V and +1.0 to +1.5 V cause an increase of the slope, indicating an increase of electrochemical kinetics.[54] The smallest slope is ascribed to the colored (−0.5 V) V_2O_5 thin films and bleached (+1.5 V) V_2O_5 films in the Zn^{2+} electrolyte, indicating the fastest electrochemical kinetics at the highest negative and positive potentials of −0.5 and +1.5 V, respectively.

Figure 1a,b shows the schematic illustration and *ex situ* optical transmittance spectra and digital photographs of the flexible ZPEM/V_2O_5/ITO EESDs in various colored and bleached states of −0.5 to +2.0 V. The high optical transmittance modulation (ΔT) of the coloration/bleaching state is observed to be ∼57.88% at a wavelength of 700 nm, lower than the ΔT value of the V_2O_5 thin films aforementioned. The reversibly switchable multi-electrochromic characteristic of the ZPEM/V_2O_5/ITO EESDs with several colors such as greenish-blue, yellowish-green, greenish-yellow, faint-yellow, yellowish-orange, and reddish-orange is obtained, consistent with that of the V_2O_5 thin films. The CIE coordinates of these colors display an arc distribution (Figure 1c) in the CIE XY between (0.50, 0.47) and (0.40, 0.49). Figure 1d shows the plot of the optical density variation (ΔOD) in relation to charge density (Q) at 633 nm of the ZPEM/V_2O_5/ITO EESDs. The CE can be determined to be 36.91 cm^2 C^{-1}, comparable to the sandwich configuration (fluorine-doped tin oxide (FTO)/WO_3/Li^+-based gelatin-based solid electrolyte/NiO/FTO) in the previous report.[25] In fact, the electrochemical and electrochromic properties of thin films and microcrystalline precipitates of V_2O_5 are strongly dependent on the method of their fabrication and experimental conditions. For instance, an atmospheric pressure chemical vapor deposited V_2O_5 thin film with a crystalline structure is reported to possess an ultrahigh coloration efficiency of 336 cm^2 C^{-1}.[55] Another example is that an electrodeposited V_2O_5 with an amorphous structure has a high coloration efficiency of 28 cm^2 C^{-1},[56] close to the value obtained in this work. The data reported here appear to support the assumption that the coloration efficiency is given for the wavelength at which it reaches its maximum value, 550 nm (highest sensitivity of the human eye) and photopic transmittance.[57,58] It seems that a selected wavelength of 633 nm for *in situ* time-dependent optical transmittance spectra meets a predetermined criterion on the basis of these results of *ex situ* transmission spectra of the V_2O_5 thin films (Figure 1b). The GCD curves with different current densities from 75 to 125 μA cm^{-2} of the

https://doi.org/10.1021/acsaem.1c02508
ACS Appl. Energy Mater. 2022, 5, 88−97

ZPEM/V_2O_5/ITO EESDs are presented in Figure 1e. It is demonstrated that all of the curves have a nonideal sloped shape, indicating a typical capacitive behavior, consistent with the pseudocapacitive performance of the V_2O_5 thin films. Therefore, the ZPEM/V_2O_5/ITO EESDs can be considered as electrochromic pseudocapacitors. As the current density increases from 0.075 to 0.125 mA cm^{-2}, the specific capacitance decreases from 51 to 28 μF cm^{-2}, indicating a superior rate performance. Moreover, the specific energy density and power density of the ZPEM/V_2O_5/ITO EESDs are, respectively, calculated based on the GCD curves, which generates the maximum peak values (where I = 0.075 mA cm^{-2} and C_s = 12.29 mF cm^{-2} in Section S2) of 12.54 μWh cm^{-2} and 1.67 mW cm^{-2}. A possible explanation for these results may be attributed to the layered structure of the V_2O_5 thin films, bivalent zinc ion intercalation/deintercalation, and excellent conductivity of the free-standing ZPEM. Interestingly, this rather contradictory result (a high energy storage capability and a small specific capacitance) may be due to the limited ionic conductivity of the Zn^{2+}-based polymeric electrolyte membrane, preventing the device from reaching its full potential, but nevertheless providing improved functionality. The effectiveness of the dual-ion Zn^{2+}/Al^{3+} hydrogel electrolyte has been exemplified in a report by Eric et al.[59] The aforementioned results demonstrate that the flexible ZPEM/V_2O_5/ITO EESDs with the simplest configuration (only the trilayer: ion conductor, electrochromic layer, and transparent conducting layer) are highly desirable for the potential applications. Another interesting feature of the flexible ZPEM/V_2O_5/ITO EESDs is the function of energy storage and release derived from zinc ion intercalation and deintercalation, as presented in Figure 1f,g. The open-circuit voltage of a couple of the fully bleached (+2.0 V) ZPEM/V_2O_5/ITO EESDs in series is measured to be ∼3.22 V (Figure S2a), which can light up a 3.0-V-rated light-emitting diode (LED). The green LED is brightest when powered by the fully bleached (+2.0 V) devices (Figure 1f), and then turned off (Figure S2b) after about 30 s, which corresponds to the discharging process of a fully charged battery state, indicating that the EESDs based on zinc ion intercalation and deintercalation are exhausted. After applying the bleached voltage (+2.0 V), the ZPEM/V_2O_5/ITO EESDs are charged and able to light up the green LED again, indicating that the devices possess a reversible charge/discharge characteristic, like supercapacitors and batteries.[60] Moreover, our device possesses a long-term cyclic stability with a capacitance retention of 82.25% after 2000 continuous cycles under a current density of 0.5 mA cm^{-2}, as depicted in Figure S3. To further present the aforementioned long-term-stable performance of the ZPEM/V_2O_5/ITO EESDs, a comparison between our devices and some other reported ECDs is summarized in Table S4, exhibiting the competitivity of our design in terms of electrochromic performance and the long-term cyclic stability.

CONCLUSIONS

In summary, the system of the two-mode Zn^{2+}/V_2O_5 active interfaces based on the liquid $Zn(CF_3SO_3)_2$-PC electrolyte and quasi-solid Zn^{2+}-based polymeric electrolyte membrane (ZPEM) was established. Evolution of the interlayer spacing, V−O-related bonds, and chemical compositions of the V_2O_5 thin films with zinc ion intercalation and deintercalation is quantitatively traced. The layered and nanocrystal-in-glass V_2O_5 thin films with zinc ion intercalation and deintercalation show the multicolor electrochromic characteristic and the pseudocapacitive feature. Identifying highly reversible redox switching of electrochromic and energy storage functions of zinc ion intercalation into and deintercalation from the host V_2O_5 electrodes allows us to fabricate the flexible ZPEM/V_2O_5/ITO EESDs with a large color contrast (multicolor electrochromism: greenish-blue, yellowish-green, greenish-yellow, faint-yellow, yellowish-orange, and reddish-orange), a large transmittance modulation of 57.88%, a high coloration efficiency of 36.91 cm^2 C^{-1}, a superior rate capacity, and an excellent pseudocapacitive feature. The large optical modulation and high-density energy storage make flexible ZPEM/V_2O_5/ITO EESDs an attractive candidate for low-cost, environmentally friendly, and bifunctional electrochromic devices.

ASSOCIATED CONTENT

Supporting Information

The Supporting Information is available free of charge at https://pubs.acs.org/doi/10.1021/acsaem.1c02508.

Structural and morphological characterizations and quantitative analysis table and digital photographs (PDF)

AUTHOR INFORMATION

Corresponding Authors

Hongliang Zhang − *Laboratory of Advanced Nano Materials and Devices, Ningbo Institute of Materials Technology and Engineering, Chinese Academy of Sciences, Ningbo 315201, P. R. China; Center of Materials Science and Optoelectronics Engineering, University of Chinese Academy of Sciences, Beijing 100049, P. R. China;* orcid.org/0000-0002-9295-8683; Email: zhanghl@nimte.ac.cn

Hongtao Cao − *Laboratory of Advanced Nano Materials and Devices, Ningbo Institute of Materials Technology and Engineering, Chinese Academy of Sciences, Ningbo 315201, P. R. China; Center of Materials Science and Optoelectronics Engineering, University of Chinese Academy of Sciences, Beijing 100049, P. R. China*; Email: h_cao@nimte.ac.cn

Authors

Chunjian Wang − *Laboratory of Advanced Nano Materials and Devices, Ningbo Institute of Materials Technology and Engineering, Chinese Academy of Sciences, Ningbo 315201, P. R. China; Center of Materials Science and Optoelectronics Engineering, University of Chinese Academy of Sciences, Beijing 100049, P. R. China*

Xinlei Zhang − *Laboratory of Advanced Nano Materials and Devices, Ningbo Institute of Materials Technology and Engineering, Chinese Academy of Sciences, Ningbo 315201, P. R. China; School of Microelectronics, Shandong University, Jinan 250100, P. R. China*

Sheng Liu − *Laboratory of Advanced Nano Materials and Devices, Ningbo Institute of Materials Technology and Engineering, Chinese Academy of Sciences, Ningbo 315201, P. R. China*

Qiang Wang − *Ningbo Wakan Electronic Science Technology Co. LTD, Ningbo 315475, P. R. China*

Chengli Zhang − *Ningbo Wakan Electronic Science Technology Co. LTD, Ningbo 315475, P. R. China*

Junhua Gao − *Laboratory of Advanced Nano Materials and Devices, Ningbo Institute of Materials Technology and*

https://doi.org/10.1021/acsaem.1c02508
ACS Appl. Energy Mater. 2022, 5, 88−97

Engineering, Chinese Academy of Sciences, Ningbo 315201, P. R. China

Lingyan Liang − *Laboratory of Advanced Nano Materials and Devices, Ningbo Institute of Materials Technology and Engineering, Chinese Academy of Sciences, Ningbo 315201, P. R. China;* orcid.org/0000-0002-6285-6600

Complete contact information is available at: https://pubs.acs.org/10.1021/acsaem.1c02508

Author Contributions

The manuscript was written through contributions of all authors. All authors have given approval to the final version of the manuscript.

Notes

The authors declare no competing financial interest.

■ ACKNOWLEDGMENTS

This project is supported by the National Natural Science Foundation of China (61974148) and Ningbo Science and Technology Innovation 2025 Major Special Project (2020Z002).

■ REFERENCES

(1) Wang, Z.; Wang, X.; Cong, S.; Geng, F.; Zhao, Z. Fusing electrochromic technology with other advanced technologies: A new roadmap for future development. *Mater. Sci. Eng., R* **2020**, *140*, No. 100524.

(2) Liu, L.; Diao, X.; He, Z.; Yi, Y.; Wang, T.; Wang, M.; Huang, J.; He, X.; Zhong, X.; Du, K. High-performance all-inorganic portable electrochromic Li-ion hybrid supercapacitors toward safe and smart energy storage. *Energy Storage Mater.* **2020**, *33*, 258−267.

(3) Laschuk, N. O.; Ebralidze, I. I.; Easton, E. B.; Zenkina, O. V. Systematic Design of Electrochromic Energy Storage Devices Based on Metal−Organic Monolayers. *ACS Appl. Energy Mater.* **2021**, *4*, 3469−3479.

(4) Yang, P.; Sun, P.; Mai, W. Electrochromic energy storage devices. *Mater. Today* **2016**, *19*, 394−402.

(5) Yun, T. G.; Park, M.; Kim, D.-H.; Kim, D.; Cheong, J. Y.; Bae, J. G.; Han, S. M.; Kim, I.-D. All-transparent stretchable electrochromic supercapacitor wearable patch device. *ACS Nano* **2019**, *13*, 3141−3150.

(6) Kim, S. Y.; Yun, T. Y.; Yu, K. S.; Moon, H. C. Reliable, high-performance electrochromic supercapacitors based on metal-doped nickel oxide. *ACS Appl. Mater. Interfaces* **2020**, *12*, 51978−51986.

(7) Raza, W.; Ali, F.; Raza, N.; Luo, Y.; Kim, K.-H.; Yang, J.; Kumar, S.; Mehmood, A.; Kwon, E. E. Recent advancements in supercapacitor technology. *Nano Energy* **2018**, *52*, 441−473.

(8) Ge, P.; Li, S.; Shuai, H.; Xu, W.; Tian, Y.; Yang, L.; Zou, G.; Hou, H.; Ji, X. Engineering 1D chain-like architecture with conducting polymer towards ultra-fast and high-capacity energy storage by reinforced pseudo-capacitance. *Nano Energy* **2018**, *54*, 26−38.

(9) Zhang, Y.; Jing, X.; Wang, Q.; Zheng, J.; Jiang, H.; Meng, C. Three-dimensional porous V_2O_5 hierarchical spheres as a battery-type electrode for a hybrid supercapacitor with excellent charge storage performance. *Dalton Trans.* **2017**, *46*, 15048−15058.

(10) Duay, J.; Gillette, E.; Liu, R.; Lee, S. B. Highly flexible pseudocapacitor based on freestanding heterogeneous MnO_2/conductive polymer nanowire arrays. *Phys. Chem. Chem. Phys.* **2012**, *14*, 3329−3337.

(11) Lee, S.-H.; Tracy, C. E.; Yan, Y.; Pitts, J. R.; Deb, S. K. Solid-State Nanocomposite Electrochromic Pseudocapacitors. *Electrochem. Solid-State Lett.* **2005**, *8*, A188.

(12) Reddy, B. N.; Kumar, P. N.; Deepa, M. A poly(3,4-ethylenedioxypyrrole)-Au@WO_3-based electrochromic pseudocapacitor. *ChemPhysChem* **2015**, *16*, 377−389.

(13) Wang, H.; Yao, C.-J.; Nie, H.-J.; Yang, L.; Mei, S.; Zhang, Q. Recent progress in integrated functional electrochromic energy storage devices. *J. Mater. Chem. C* **2020**, *8*, 15507−15525.

(14) Zhang, W.; Li, H.; Al-Hussein, M.; Elezzabi, A. Y. Electrochromic Battery Displays with Energy Retrieval Functions Using Solution-Processable Colloidal Vanadium Oxide Nanoparticles. *Adv. Opt. Mater.* **2020**, *8*, No. 1901224.

(15) Ming, F.; Liang, H.; Lei, Y.; Kandambeth, S.; Eddaoudi, M.; Alshareef, H. N. Layered $Mg_xV_2O_5{\cdot}nH_2O$ as Cathode Material for High-Performance Aqueous Zinc Ion Batteries. *ACS Energy Lett.* **2018**, *3*, 2602−2609.

(16) He, P.; Zhang, G.; Liao, X.; Yan, M.; Xu, X.; An, Q.; Liu, J.; Mai, L. Sodium ion stabilized vanadium oxide nanowire cathode for high-performance zinc-ion batteries. *Adv. Energy Mater.* **2018**, *8*, No. 1702463.

(17) Kundu, D.; Adams, B. D.; Duffort, V.; Vajargah, S. H.; Nazar, L. F. A high-capacity and long-life aqueous rechargeable zinc battery using a metal oxide intercalation cathode. *Nat. Energy* **2016**, *1*, No. 16119.

(18) Xia, C.; Guo, J.; Li, P.; Zhang, X.; Alshareef, H. N. Highly stable aqueous zinc-ion storage using layered calcium vanadium oxide bronze cathode. *Angew. Chem., Int. Ed.* **2018**, *57*, 3943−3948.

(19) Cong, S.; Geng, F.; Zhao, Z. Tungsten oxide materials for optoelectronic applications. *Adv. Mater.* **2016**, *28*, 10518−10528.

(20) Li, K.; Shao, Y.; Liu, S.; Zhang, Q.; Wang, H.; Li, Y.; Kaner, R. B. Aluminum-Ion-Intercalation Supercapacitors with Ultrahigh Areal Capacitance and Highly Enhanced Cycling Stability: Power Supply for Flexible Electrochromic Devices. *Small* **2017**, *13*, No. 1700380.

(21) Lin, M. C.; Gong, M.; Lu, B.; Wu, Y.; Wang, D. Y.; Guan, M.; Angell, M.; Chen, C.; Yang, J.; Hwang, B. J.; Dai, H. An ultrafast rechargeable aluminium-ion battery. *Nature* **2015**, *520*, 324.

(22) Qiu, D.; Ji, H.; Zhang, X.; Zhang, H.; Cao, H.; Chen, G.; Tian, T.; Chen, Z.; Guo, X.; Liang, L.; Gao, J.; Zhuge, F. Electrochromism of Nanocrystal-in-Glass Tungsten Oxide Thin Films under Various Conduction Cations. *Inorg. Chem.* **2019**, *58*, 2089−2098.

(23) Chen, G.; Wang, Y.; Pei, Z. Adsorption and desorption of 2,4,6-trichlorophenol onto and from ash as affected by Ag^+, Zn^{2+}, and Al^{3+}. *Environ. Sci. Pollut. Res.* **2014**, *21*, 2002−2008.

(24) Yan, M.; He, P.; Chen, Y.; Wang, S.; Wei, Q.; Zhao, K.; Xu, X.; An, Q.; Shuang, Y.; Shao, Y.; Mueller, K. T.; Mai, L.; Liu, J.; Yang, J. Water-Lubricated Intercalation in $V_2O_5.nH_2$ O for High-Capacity and High-Rate Aqueous Rechargeable Zinc Batteries. *Adv. Mater.* **2018**, *30*, No. 1703725.

(25) Ramadan, R.; Kamal, H.; Hashem, H. M.; Abdel-Hady, K. Gelatin-based solid electrolyte releasing Li^+ for smart window applications. *Sol. Energy Mater. Sol. Cells* **2014**, *127*, 147−156.

(26) Llordés, A.; Garcia, G.; Gazquez, J.; Milliron, D. J. Tunable near-infrared and visible-light transmittance in nanocrystal-in-glass composites. *Nature* **2013**, *500*, 323−326.

(27) Wang, L.; Guo, M.; Zhan, J.; Jiao, X.; Chen, D.; Wang, T. A new design of an electrochromic energy storage device with high capacity, long cycle lifetime and multicolor display. *J. Mater. Chem. A* **2020**, *8*, 17098−17105.

(28) Xie, S.; Bi, Z.; Chen, Y.; He, X.; Guo, X.; Gao, X.; Li, X. Electrodeposited Mo-doped WO_3 film with large optical modulation and high areal capacitance toward electrochromic energy-storage applications. *Appl. Surf. Sci.* **2018**, *459*, 774−781.

(29) Jin, A.; Chen, W.; Zhu, Q.; Yang, Y.; Volkov, V. L.; Zakharova, G. S. Structural and electrochromic properties of molybdenum doped vanadium pentoxide thin films by sol−gel and hydrothermal synthesis. *Thin Solid Films* **2009**, *517*, 2023−2028.

(30) Guan, S.; Wei, Y.; Zhou, J.; Zheng, J.; Xu, C. A Method for Preparing Manganese-Doped V_2O_5 Films with Enhanced Cycling Stability. *J. Electrochem. Soc.* **2016**, *163*, H541−H545.

(31) Liu, Y.; Clark, M.; Zhang, Q.; Yu, D.; Liu, D.; Liu, J.; Cao, G. V_2O_5 Nano-Electrodes with High Power and Energy Densities for Thin Film Li-Ion Batteries. *Adv. Energy Mater.* **2011**, *1*, 194−202.

(32) Zhang, X.; Sun, H.; Li, Z.; Xu, J.; Jiang, S.; Zhu, Q.; Jin, A.; Zakharova, G. S. Synthesis and electrochromic characterization of

vanadium pentoxide/graphene nanocomposite films. *J. Electrochem. Soc.* **2013**, *160*, H587−H590.
(33) Zhang, L.; Chen, L.; Zhou, X.; Liu, Z. Towards High-Voltage Aqueous Metal-Ion Batteries Beyond 1.5 V: The Zinc/Zinc Hexacyanoferrate System. *Adv. Energy Mater.* **2015**, *5*, No. 1400930.
(34) Jia, Z.; Wang, B.; Wang, Y. Copper hexacyanoferrate with a well-defined open framework as a positive electrode for aqueous zinc ion batteries. *Mater. Chem. Phys.* **2015**, *149*−*150*, 601−606.
(35) Wu, J.; Qiu, D.; Zhang, H.; Cao, H.; Wang, W.; Liu, Z.; Tian, T.; Liang, L.; Gao, J.; Zhuge, F. Flexible electrochromic V_2O_5 thin films with ultrahigh coloration efficiency on graphene electrodes. *J. Electrochem. Soc.* **2018**, *165*, D183.
(36) Rama, N.; Ramachandra Rao, M. S. Synthesis and study of electrical and magnetic properties of vanadium oxide micro and nanosized rods grown using pulsed laser deposition technique. *Solid State Commun.* **2010**, *150*, 1041−1044.
(37) Manning, T. D.; Parkin, I. P. Vanadium(IV) oxide thin films on glass and silicon from the atmospheric pressure chemical vapour deposition reaction of $VOCl_3$ and water. *Polyhedron* **2004**, *23*, 3087−3095.
(38) Dultsev, F. N.; Vasilieva, L. L.; Maroshina, S. M.; Pokrovsky, L. D. Structural and optical properties of vanadium pentoxide sol−gel films. *Thin Solid Films* **2006**, *510*, 255−259.
(39) Mjejri, I.; Etteyeb, N.; Sediri, F. Hydrothermal synthesis of mesoporous rod-like nanocrystalline vanadium oxide hydrate $V_3O_7 \cdot H_2O$ from hydroquinone and V_2O_5. *Mater. Res. Bull.* **2013**, *48*, 3335−3341.
(40) Jin, A.; Chen, W.; Zhu, Q.; Jian, Z. Multi-electrochromism behavior and electrochromic mechanism of electrodeposited molybdenum doped vanadium pentoxide films. *Electrochim. Acta* **2010**, *55*, 6408−6414.
(41) Zhao, G.-f.; Wang, W.-q.; Wang, X.-l.; Xia, X.-h.; Gu, C.-d.; Tu, J.-p. A multicolor electrochromic film based on a SnO_2/V_2O_5 core/shell structure for adaptive camouflage. *J. Mater. Chem. C* **2019**, *7*, 5702−5709.
(42) Li, Y.; Huang, Z.; Kalambate, P. K.; Zhong, Y.; Huang, Z.; Xie, M.; Shen, Y.; Huang, Y. V_2O_5 nanopaper as a cathode material with high capacity and long cycle life for rechargeable aqueous zinc-ion battery. *Nano Energy* **2019**, *60*, 752−759.
(43) Zhou, J.; Shan, L.; Wu, Z.; Guo, X.; Fang, G.; Liang, S. Investigation of V_2O_5 as a low-cost rechargeable aqueous zinc ion battery cathode. *Chem. Commun.* **2018**, *54*, 4457−4460.
(44) Yang, P.; Sun, P.; Du, L.; Liang, Z.; Xie, W.; Cai, X.; Huang, L.; Tan, S.; Mai, W. Quantitative Analysis of Charge Storage Process of Tungsten Oxide that Combines Pseudocapacitive and Electrochromic Properties. *J. Phys. Chem. C* **2015**, *119*, 16483−16489.
(45) Zhao, B.; Lu, S.; Zhang, X.; Wang, H.; Liu, J.; Yan, H. Porous WO_3/reduced graphene oxide composite film with enhanced electrochromic properties. *Ionics* **2016**, *22*, 261−267.
(46) Qin, T.; Dang, S.; Hao, J.; Wang, Z.; Li, H.; Wen, Y.; Lu, S.; He, D.; Cao, G.; Peng, S. Carbon fabric supported 3D cobalt oxides/hydroxide nanosheet network as cathode for flexible all-solid-state asymmetric supercapacitor. *Dalton Trans.* **2018**, *47*, 11503−11511.
(47) Yu, X.; Yun, S.; Yeon, J. S.; Bhattacharya, P.; Wang, L.; Lee, S. W.; Hu, X.; Park, H. S. Emergent Pseudocapacitance of 2D Nanomaterials. *Adv. Energy Mater.* **2018**, *8*, No. 1702930.
(48) Zhang, L.; Miao, L.; Zhang, B.; Wang, J.; Liu, J.; Tan, Q.; Wan, H.; Jiang, J. A durable VO_2(M)/Zn battery with ultrahigh rate capability enabled by pseudocapacitive proton insertion. *J. Mater. Chem. A* **2020**, *8*, 1731−1740.
(49) Wei, Y. X.; Ma, Y. B.; Chen, M.; Liu, W. M.; Li, L.; Yan, Y. Electrochemical investigation of electrochromic device based on WO_3 and Ti doped V_2O_5 films by using electrolyte containing ferrocene. *J. Electroanal. Chem.* **2017**, *807*, 45−51.
(50) Chandra, M. V. L.; Karthikeyan, S.; Selvasekarapandian, S.; Pandi, D. V.; Monisha, S.; Packiaseeli, S. A. Characterization of high ionic conducting PVAc−PMMA blend-based polymer electrolyte for electrochemical applications. *Ionics* **2016**, *22*, 2409−2420.
(51) Schneider, K.; Dziubaniuk, M.; Wyrwa, J. Impedance Spectroscopy of Vanadium Pentoxide Thin Films. *J. Electron. Mater.* **2019**, *48*, 4085−4091.
(52) Le, S.; Wen, S.; Zou, Z.; Li, Y. Effect of La Doping on the Structure and Lithium Storage Performance of V_2O_5. *J. Nanosci. Nanotechnol.* **2019**, *19*, 7421−7426.
(53) Ray, A.; Roy, A.; Bhattacharjee, S.; Jana, S.; Ghosh, C. K.; Sinha, C.; Das, S. Correlation between the dielectric and electrochemical properties of TiO_2-V_2O_5 nanocomposite for energy storage application. *Electrochim. Acta* **2018**, *266*, 404−413.
(54) Ma, Z.; Zhou, X.; Deng, W.; Lei, D.; Liu, Z. 3D Porous MXene (Ti_3C_2)/Reduced Graphene Oxide Hybrid Films for Advanced Lithium Storage. *ACS Appl. Mater. Interfaces* **2018**, *10*, 3634−3643.
(55) Vernardou, D. Using an atmospheric pressure chemical vapor deposition process for the development of V_2O_5 as an electrochromic material. *Coatings* **2017**, *7*, No. 24.
(56) He, W.; Liu, Y.; Wan, Z.; Jia, C. Electrodeposition of V_2O_5 on TiO_2 nanorod arrays and their electrochromic properties. *RSC Adv.* **2016**, *6*, 68997−69006.
(57) Kraft, A. Electrochromism: a fascinating branch of electrochemistry. *ChemTexts* **2019**, *5*, No. 1.
(58) Halder, S.; Roy, S.; Chakraborty, C. Multicolored and durable electrochromism in water soluble naphthalene and perylene based diimides. *Sol. Energy Mater. Sol. Cells* **2022**, *234*, No. 111429.
(59) Eric, H.; Li, H.; Elezzabi Adulhakem, Y. Rechargeable Zn^{2+}/Al^{3+} dual-ion electrochromic device with long life time utilizing dimethyl sulfoxide (DMSO)-nanocluster modified hydrogel electrolytes. *RSC Adv.* **2019**, *9*, 32047−32057.
(60) Zhao, J.; Tian, Y.; Wang, Z.; Cong, S.; Zhou, D.; Zhang, Q.; Yang, M.; Zhang, W.; Geng, F.; Zhao, Z. Trace H_2O_2 -Assisted High-Capacity Tungsten Oxide Electrochromic Batteries with Ultrafast Charging in Seconds. *Angew. Chem., Int. Ed.* **2016**, *55*, 7161−7165.

https://doi.org/10.1021/acsaem.1c02508
ACS Appl. Energy Mater. 2022, 5, 88−97